

## EFFECTS OF MECHANICAL COUPLING ON THE DYNAMICS OF BALANCING TASKS

KATSUTOSHI YOSHIDA

Department of Mechanical and Intelligent Engineering  
Utsunomiya University  
7-1-2 Yoto, Utsunomiya-shi, Tochigi 321-8585, Japan  
yoshidak@cc.utsunomiya-u.ac.jp

ATSUSHI HIGETA

Department of Innovation Systems Engineering  
Utsunomiya University  
higeta@katzlab.jp

SHINICHI WATANABE

Innovation Center for Research and Engineering Education  
Utsunomiya University  
swtnb@cc.utsunomiya-u.ac.jp

**ABSTRACT.** Coupled human balancing tasks are investigated based on both pseudo-neural controllers characterized by time-delayed feedback with random gain and natural human balancing tasks. It is shown numerically that, compared to single balancing tasks, balancing tasks coupled by mechanical structures exhibit enhanced stability against balancing errors in terms of both amplitude and velocity and also improve the tracking ability of the controllers. We then perform an experiment in which numerical pseudo-neural controllers are replaced with natural human balancing tasks carried out using computer mice. The results reveal that the coupling structure generates asymmetric tracking abilities in subjects whose tracking abilities are nearly symmetric in their single balancing tasks.

**Keywords:** Neural Controller, Mechanical Coupling, Visuomotor Tracking, Stability, Sensitivity

**1. Introduction.** Competitive and cooperative dynamics can arise when multiple agents (autonomous entities) share common resources and environments. Extensive research has been conducted on such mutual interactions. Research in this area can be broadly classified into two categories: the field of mathematical ecology [1], which finds group behavior models having low degrees of freedom, and the field of multi-robot systems [2], which develops individual agents generating group behavior. In these conventional approaches, couplings between agents are constructed using shared resources or information.

On the other hand, it is also reasonable to consider another type of coupling, constructed of mechanical structures, for instance, connection rods placed between agents. Such a mechanical type of coupling appears to play an important role in clarifying the dynamics of agents, including humans and robots, which are in physical contact with one another. This type of knowledge will be applicable to developing robots working together or robots supporting human activities, based on physical contact. However,

it appears that little is known about the type of dynamics that is produced by mechanical coupling. Therefore, as a preliminary step toward solving this problem, we have developed the coupled inverted pendula (CIP) model with four DOF [3], in which non-linear behavior similar to interspecific competition in an ecosystem [1] can be directly generated by individual mechanical structures of agents. The CIP model proposed by the authors consists of a pair of independently PD-controlled inverted pendula, the tips of which are connected through a rigid rod.

The primary approach used in the present study is to replace the PD controllers of the CIP model with human balancing tasks. It follows that the two subjects perform stick balancing tasks under the situation in which the tips of the sticks are mechanically connected to each other. This approach will allow us to determine how humans work together dynamically through physical contacts and will consequently provide helpful information for developing robots to support human activities.

From an engineering point of view, stick balancing is basically achieved by the tracking control technique (See References [4, 5] for typical examples in engineering problems). However, human tracking control is known to exhibit further characteristics beyond engineering tracking control. For example, the human tracking control is known to have a relatively large time-delay caused by neural latency and parametric random fluctuations typical of neural control [6]. In the field of statistical mechanics, it has been reported that random fluctuations arising in single human stick balancing tasks can be accurately modeled as an inverted pendulum with a time-delayed and randomly modulated feedback controller [6]. Since such a controller does not simulate the structure of neural networks [7, 8], it should be referred to as a pseudo-neural control model of human balancing tasks. The most remarkable effect of the pseudo-neural controller is that, near stability boundaries, parametric noise can allow the controller to produce corrective movements on time scales shorter than the delay time of the controller under certain suitable conditions, exhibiting the scaling laws typical of the self-similarity dynamics of on-off intermittency [9]. This effect has also been experimentally confirmed in regard to physical human tasks, such as stick balancing [6, 10] and visuomotor tracking on a computer screen [11]. In these studies on the human balancing task, however, the case for two coupled humans has never been considered. Although common features of human control would remain even in the coupled case, there must be specific effects related to interactions between the two humans. This problem remains to be addressed.

In the present paper, we consider the open problem of what kind of dynamics may arise when mechanical coupling is imposed on the balancing tasks by two humans whose dynamics can be characterized by the time-delayed and randomly modulated feedback controller. To achieve this, we propose a new model consisting of time-delayed and randomly modulated feedback controllers that are coupled by a mechanical structure equivalent to the proposed CIP model. For simplicity, we first derive a linearized reduced-order version of the CIP model, after which we replace the PD controllers with pseudo-neural controllers, as developed in the literature [6, 10, 11]. Using this model, we demonstrate the effects of coupling, namely, an improvement in stability and sensitivity of the corrective motions in the balancing tasks. We also perform an experiment in which we replace the numerical controllers with human visuomotor tracking tasks performed by subjects using computer mice. It is shown experimentally that the coupling structure between two subjects induces asymmetric sensitivity in the corrective motions of the subjects.



FIGURE 1. An intuitive example representing a coupled human balancing task.

## 2. Analytical Model.

**2.1. Single balancing tasks.** Human stick balancing tasks and their scaling properties have been accurately modeled as an inverted pendulum with a time-delayed feedback of random gain of the following form [6]:

$$\ddot{\theta} + \gamma \dot{\theta} - \alpha \sin \theta + \beta R(t) \theta(t - \tau) = 0 \quad (1)$$

where  $\tau$  is a time delay representing the latency of neural reflexes in human balancing tasks and  $R(t) = 1 + \nu \xi(t)$  is a random feedback gain,  $\xi(t)$  is standard Gaussian white noise, and  $\nu$  represents the strength of the noise. Note that a stick of length  $l$  and constant linear density is modeled as  $\alpha = 3g/(2l)$ , where  $g$  is the gravitational acceleration.

Assuming that  $\theta \approx \Delta x$ ,  $|\Delta x| \ll 1$ , we obtain the linearized version of (1):

$$\Delta \ddot{x} + \gamma \Delta \dot{x} - \alpha \Delta x + \beta R(t) \Delta x(t - \tau) = 0 \quad (2)$$

which can be interpreted as an equation of motion of the relative displacement  $\Delta x := x_T(t) - x_M(t)$ , where  $x_T$  is the displacement of the upper end of the stick and  $x_M$  is the displacement of the lower end of the stick in the balancing task. It has been reported [11] that  $x_T(t)$  and  $x_M(t)$  are governed by the following equations:

$$\ddot{x}_T + \gamma \dot{x}_T = \alpha \Delta x(t), \quad \ddot{x}_M + \gamma \dot{x}_M = \beta R(t) \Delta x(t - \tau). \quad (3)$$

**2.2. Coupled balancing tasks.** In the present paper, we investigate the type of stability that can arise if two subjects that can be balanced independently are linked with a mechanical structure. Figure 1 shows an intuitive example representing this situation, in which each subject manipulates one of the sticks at the lower end along a mechanical slider with the goal of maintaining the stick in the upright position. Let  $q_{Ti}$  and  $q_{Mi}$  ( $i = 1, 2$ ) be the horizontal displacement of the upper and lower ends, respectively, of the  $i$ th stick. Then, the presence of the connecting rod can be described

## The CIP model (Nonlinear 2-D)

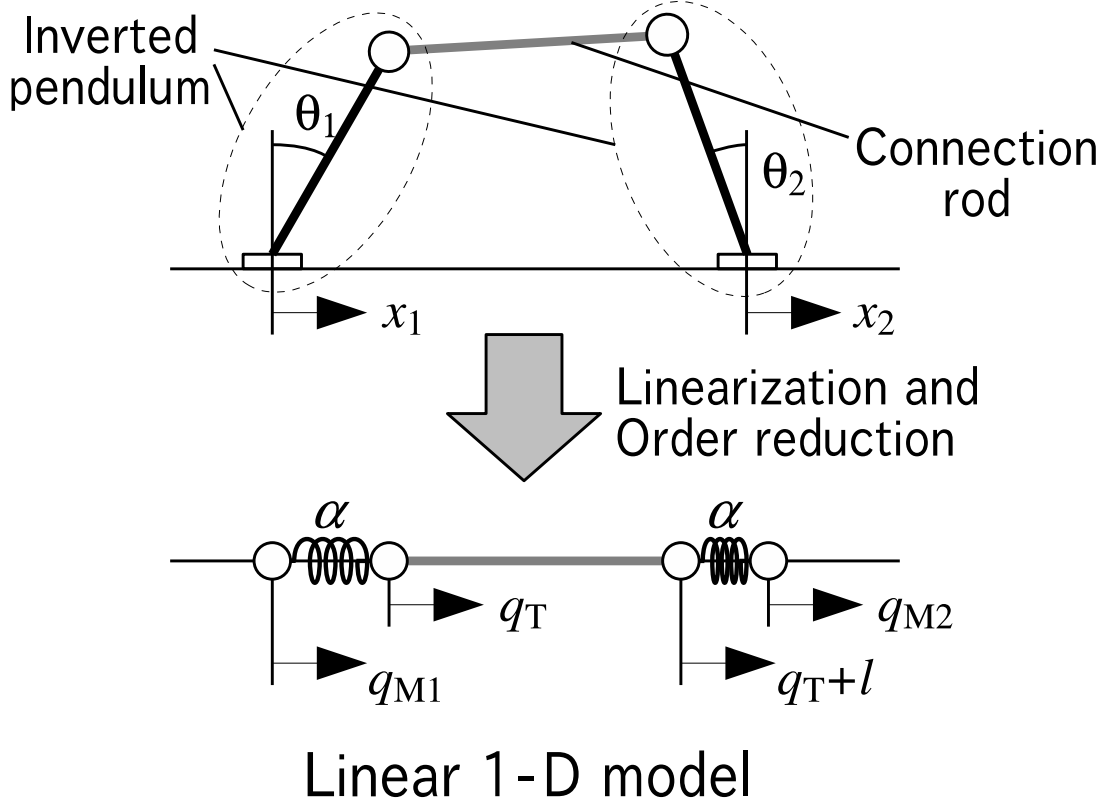


FIGURE 2. Order reduction and linearization of the CIP model.

by the distance  $l := q_{T1} - q_{T2}$  maintained by the fixed length of the rod. Note that this constant length yields the following equalities:

$$\dot{q}_{T1} = \dot{q}_{T2} =: \dot{q}_T, \quad \ddot{q}_{T1} = \ddot{q}_{T2} =: \ddot{q}_T. \quad (4)$$

For a simpler description of this coupled task, we propose the following model:

$$\begin{aligned} 2\ddot{q}_T + 2\gamma\dot{q}_T &= \alpha \Delta q_1(t) + \alpha \Delta q_2(t), \\ \ddot{q}_{Mi} + \gamma\dot{q}_{Mi} &= u_i(t, \tau), \\ u_i(t, \tau) &:= \beta R_i(t) \Delta q_i(t - \tau) \quad (i = 1, 2) \end{aligned} \quad (5)$$

where  $\Delta q_i := q_T - q_{Mi}$  ( $i = 1, 2$ ) represents the horizontal displacement between the upper and lower ends, respectively, of the  $i$ th stick, as obtained in independent balancing, and  $R_i(t) = 1 + \nu\xi_i(t)$  ( $i = 1, 2$ ) are independent random feedback gains, where  $\xi_i$  ( $i = 1, 2$ ) are mutually independent standard Gaussian white noises. The second equation of (5) can be reduced to the following relative form:

$$\Delta\ddot{q}_i + \gamma \Delta\dot{q}_i - \frac{1}{2}\alpha(\Delta q_1 + \Delta q_2) + u_i(t, \tau) = 0 \quad (i = 1, 2). \quad (6)$$

The proposed model (5) provides a linearized reduced-order counterpart of the CIP model [3], as shown schematically in Fig.2. In other words, by assuming  $|\theta_i| \ll 1$ , the gravitational restoring force proportional to  $\sin \theta_i$  in the CIP model is approximated as a linear spring force with a negative coefficient  $\alpha < 0$ . This setup is expected to

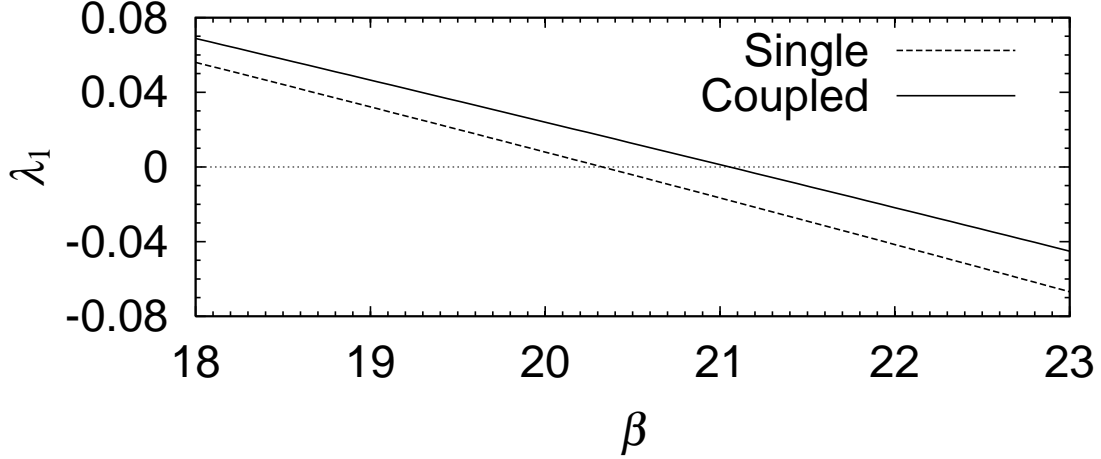


FIGURE 3. Largest Lyapunov exponent  $\lambda_1$  for the single and coupled balancing tasks as a function of the feedback gain  $\beta$ .

provide the simplest model of coupled human balancing tasks. Note that the coupled model (6) coincides with the single model (2) if  $\Delta q_1 = \Delta q_2$  and  $\Delta \dot{q}_1 = \Delta \dot{q}_2$ . In the following, we choose  $\gamma = 50$ ,  $\alpha = 22$ ,  $\nu = 0.6$ , and  $\tau = 0.1$ . For convenience, we refer to  $\Delta x$  and  $\Delta q_i$  as *balancing errors*.

The linearized model (5) conserves the essential instability of the stick in the upright position originally described in (1). Although this linear approximation becomes invalid as the balancing errors  $\Delta x$  and  $\Delta q_i$  increase, these errors remain sufficiently small during the balancing task of maintaining the stick near the upright position.

### 3. Effects of Coupling in the Balancing Model.

**3.1. On-off intermittency.** The human stick balancing task exhibits on-off intermittency with respect to the balancing error [6, 11], and the on-off intermittency occurs when the largest Lyapunov exponent  $\lambda_1$  is slightly larger than zero [9]. Letting  $\mathbf{q} = (q_1, \dot{q}_1, q_2, \dot{q}_2)$  be the solution of (5) and letting  $\Delta \mathbf{q}$  be the infinitesimal distance from the equilibrium point, we obtain the largest Lyapunov exponent  $\lambda_1$  defined by [9],

$$\lambda_1 = \lim_{t \rightarrow \infty} \frac{1}{t} \log \|\Delta \mathbf{q}(t)\| \quad (7)$$

where  $\|\Delta \mathbf{q}\|$  represents a Euclid norm of the vector  $\Delta \mathbf{q}$ .

Figure 3 shows the largest Lyapunov exponent  $\lambda_1$  of  $\Delta x$  and  $\Delta q_1$  as numerically calculated from (2) and (5), respectively. The results for  $\Delta q_2$  are omitted due to their similarity to the results for  $\Delta q_1$ . We choose  $\lambda_1 = 5 \times 10^{-5}$  to be slightly larger than zero in order to produce on-off intermittency of the balancing errors  $\Delta x$  in (2) and  $\Delta q_1$  in (5), as shown in Fig.4.

Figures 5(a) and 5(b) show double logarithmic plots of the power spectra of the balancing errors  $\Delta x$  and  $\Delta q_1$ , respectively. The results for  $\Delta q_2$  are omitted due to their similarity to the results for  $\Delta q_1$ . Both results have two linear slopes representing two power law regimes, which is in good agreement with previous balancing experiments [6, 10, 11], in which the two slopes were interpreted as a sign of on-off intermittency [9]. Based on these results, it can be concluded that the coupling term does not change the scaling law typical of the on-off intermittency of balancing tasks.

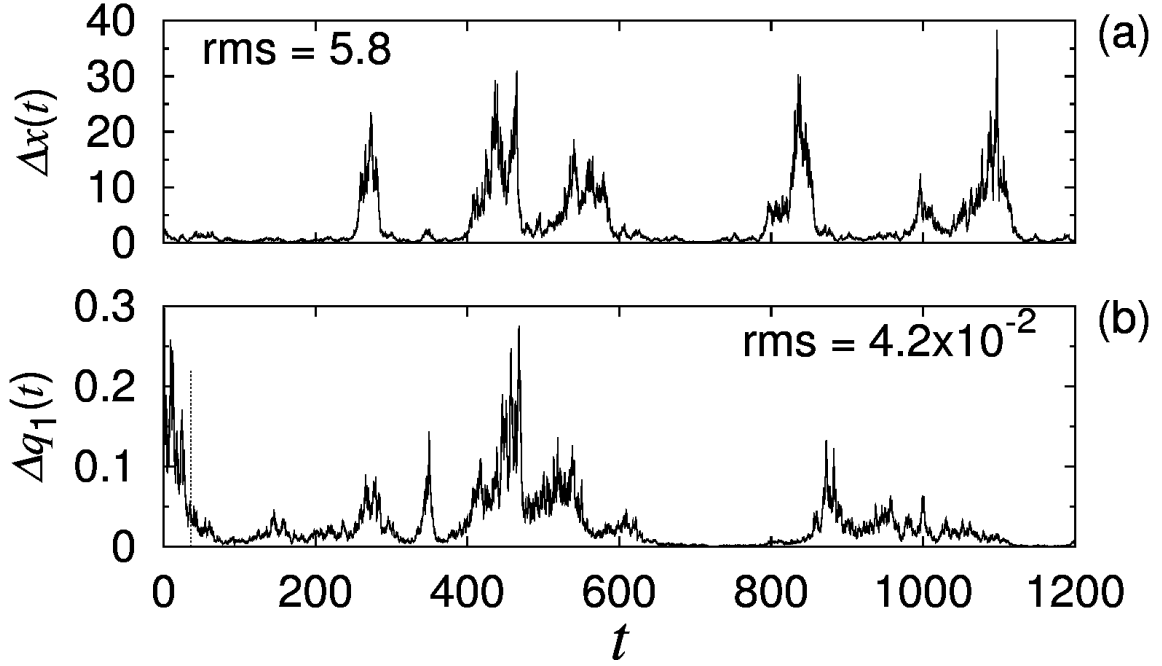


FIGURE 4. Balancing error  $\Delta x(t)$  of the single system (2) for  $\lambda_1 = 5 \times 10^{-4}$  ( $\beta = 20.306$ ) and  $\Delta q_1(t)$  of the coupled system (5) for  $\lambda_1 = 5 \times 10^{-4}$  ( $\beta = 21.032$ ).

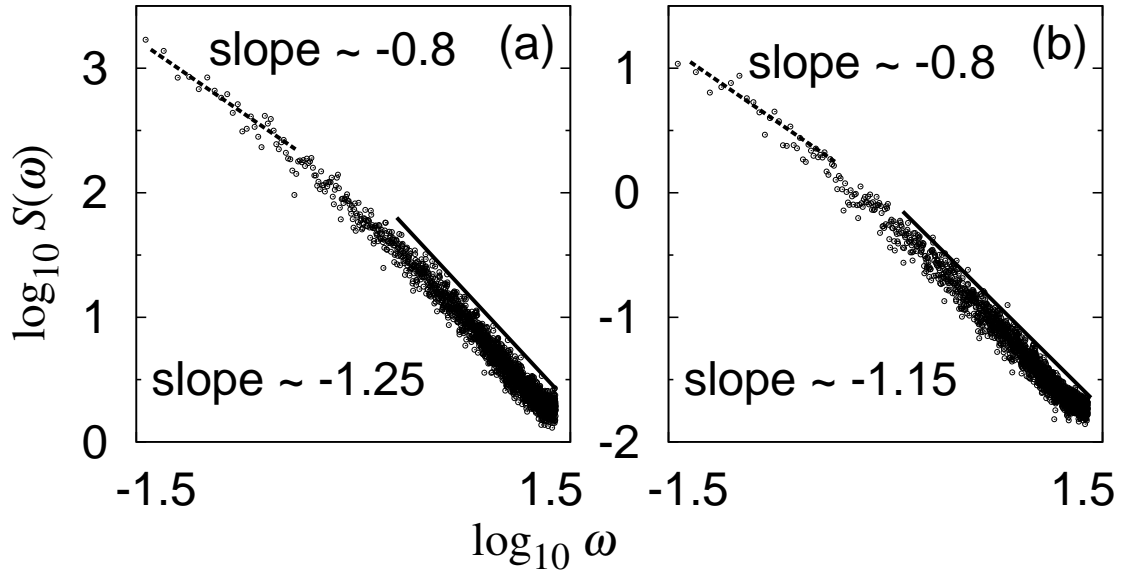


FIGURE 5. Scaling laws in the power spectra of (a) the single balancing task in (2) for  $\lambda_1 = 5 \times 10^{-4}$  ( $\beta = 20.306$ ) and (b) the coupled balancing task in (5) for  $\lambda_1 = 5 \times 10^{-4}$  ( $\beta = 21.032$ ).

**3.2. Coupling-induced stability.** The most remarkable effect of the coupling in (5) is that the balancing error is drastically suppressed by the coupling, as shown in Figs. 4(a) and 4(b). In other words, the error  $\Delta q_1$  for coupled balancing is as low as 1%

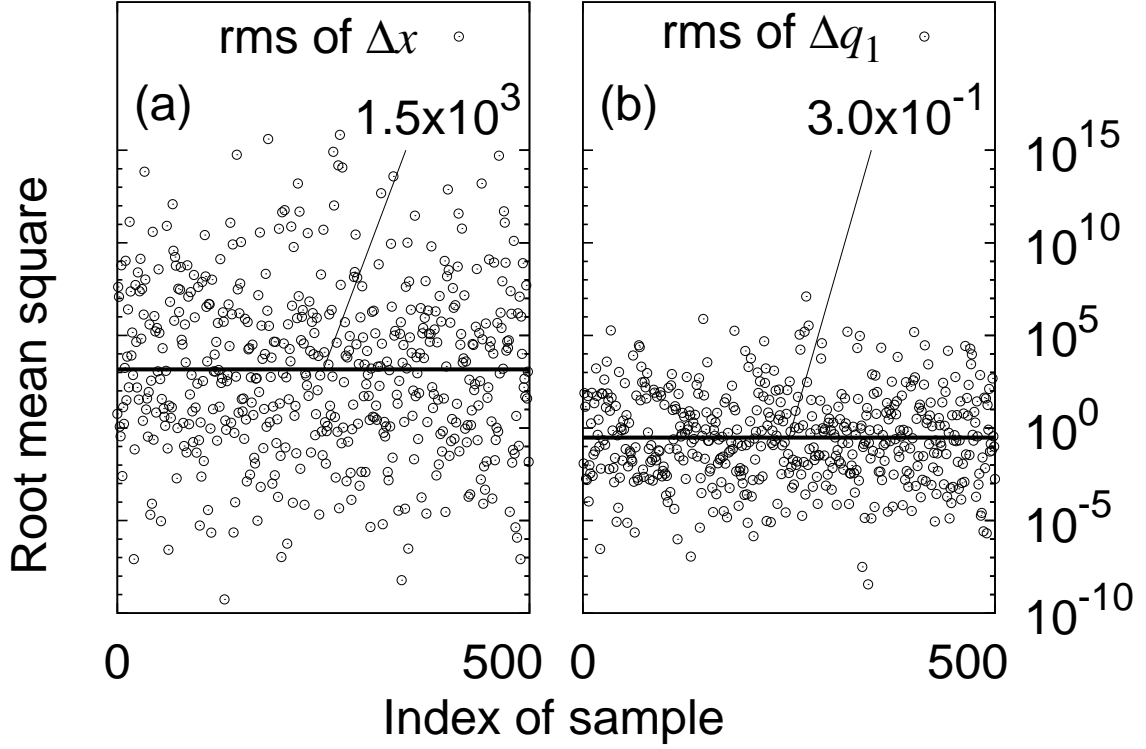


FIGURE 6. Logarithmic plot of the root mean squares of balancing error generated by different samples of the white noise  $\xi_i(t)$ . Solid lines represent the respective mean values of the logarithmic plots.

of  $\Delta x$  of that of single balancing in terms of both maximal values and root mean square (RMS) values. Figure 6 shows logarithmic plots of 500 realizations of the RMS values. The mean RMS values, represented by the solid lines, are  $1.5 \times 10^3$  for single balancing and  $3.0 \times 10^{-1}$  for coupled balancing. The results for  $\Delta q_2$  are omitted due to their similarity to those for  $\Delta q_1$ . Figure 6 shows that the coupling term reduces the balancing error  $\Delta q_1(t)$  to 0.02% of  $\Delta x$  for single balancing. This result implies that the mechanical coupling structure can improve the stability of the amplitude in human balancing tasks.

In order to examine the velocities of the balancing errors, the ratio of the probability density  $p(\Delta \dot{q}_1)$  divided by  $p(\Delta \dot{x})$  is shown in Fig.7, where  $\Delta \dot{q}_1$  and  $\Delta \dot{x}$  are the velocity errors for the coupled balancing and the single balancing tasks, respectively. Figure 7 shows that  $p(\Delta \dot{q}_1)$  is approximately twice as high as  $p(\Delta \dot{x})$  near the origin. Since, in the linear approximation, the velocity errors  $\Delta \dot{x}$  and  $\Delta \dot{q}_i$  are proportional to the respective slant angles of the sticks, the results suggest that the probability of maintaining constant angles is nearly doubled by the mechanical coupling structure.

Based on these results, the mechanical coupling structure may reduce the balancing error in terms of both amplitude and velocity under suitable conditions. Although it is beyond the scope of the present study, one possible explanation of this coupling-induced stability might be that the coupling causes some stochastic averaging effect, whereby the two independent fluctuations  $\xi_i(t)$  ( $i = 1, 2$ ) cancel each other through the coupling constraint. This canceling process, however, occurs in a stochastic manner

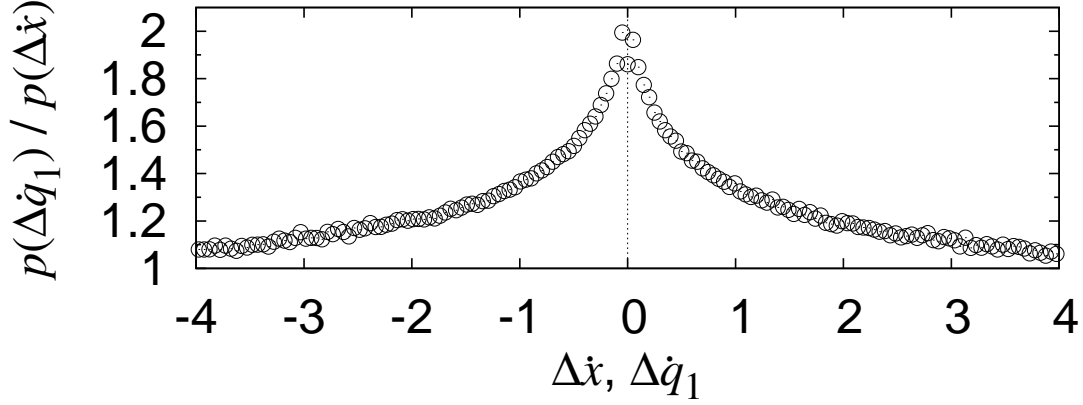


FIGURE 7. Ratio of the respective probability densities of the velocities  $\Delta\dot{q}_1$  and  $\Delta\dot{x}$  for coupled and single balancing.

so that further stochastic analysis related to the noise-induced order [12] in the field of statistical physics will be helpful in explaining the coupling-induced stability.

**3.3. Coupling-induced sensitivity.** It has been reported that near stability boundaries, parametric noise can allow time-delayed feedback controllers to produce corrective movements on a time scale shorter than that of the delayed feedback [6]. In order to observe the effect of this improvement in sensitivity as a function of time, we consider the short-time cross-correlation coefficient (STCC) in the following manner. Letting  $x(t), y(t)$  be a pair of time series to be compared and letting  $\Delta t$  be the length of the time interval of short-time averaging, we define the STCC as follows:

$$R(x, y; \tau)(t) = \frac{C(x - m_x, y - m_y; \tau, t)}{\sigma_x \sigma_y}, \quad (8)$$

where

$$C(x, y; \tau, t) := \langle x(s)y(s + \tau) \rangle_{[t, t + \Delta t]},$$

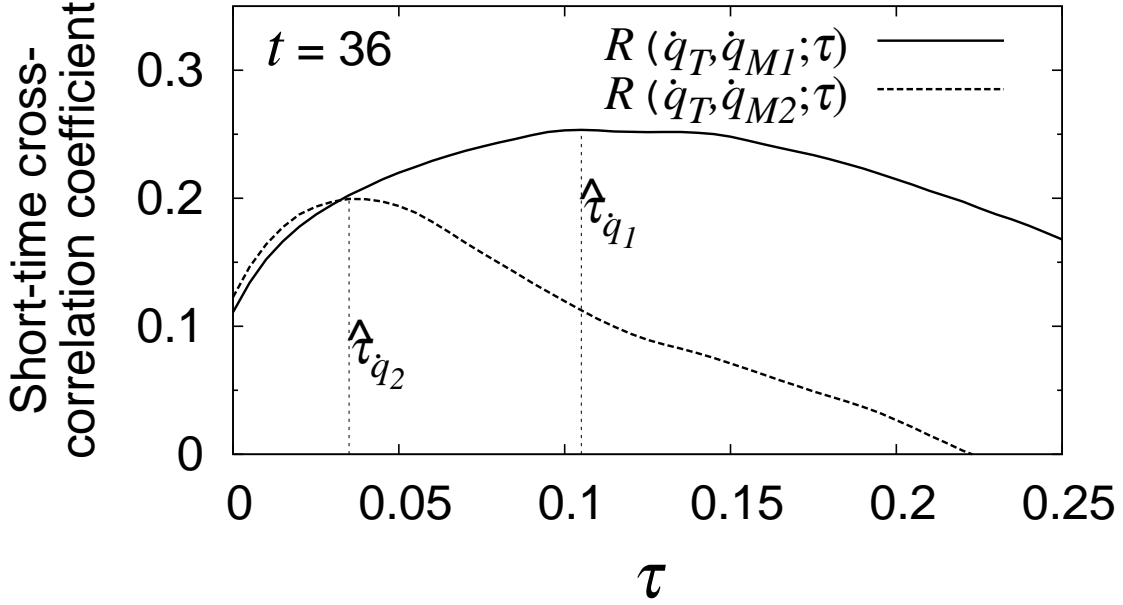
$$m_x := \langle x(s) \rangle_{[t, t + \Delta t]}, \quad \sigma_x := \langle (x(s) - m_x)^2 \rangle_{[t, t + \Delta t]}^{1/2}$$

where  $\langle X(s) \rangle_{[a, b]} := (b - a)^{-1} \int_a^b X(s) ds$  is the temporal average of  $X(s)$  over the time interval  $[a, b]$ .

In the following, we draw a comparison between the velocities of the upper end and the lower end of each stick by using the STCC in (8). More specifically, we focus on  $R(\dot{x}_T, \dot{x}_M)$  for the single system (3) and  $R(\dot{q}_T, \dot{q}_{M1})$  ( $i = 1, 2$ ) for the coupled system (5). Moreover, in order to evaluate the sensitivity of the corrective movements of the feedback controllers, we also define the first dominant peak points  $\hat{\tau}_{\dot{x}}$ ,  $\hat{\tau}_{\dot{q}_1}$ , and  $\hat{\tau}_{\dot{q}_2}$  in  $R(\dot{x}_T, \dot{x}_M)$  and  $R(\dot{q}_T, \dot{q}_{Mi})$  ( $i = 1, 2$ ). These peak points are assumed to evaluate the *tracking abilities* of the feedback controllers.

Figure 8 shows the realization of the STCCs,  $R(\dot{q}_T, \dot{q}_{M1})$  and  $R(\dot{q}_T, \dot{q}_{M2})$  of the coupled system (5) at  $t = 36$  for  $\Delta t = 5$ . In this plot, there are single peaks at  $\hat{\tau}_{\dot{q}_1} = 0.105$  and  $\hat{\tau}_{\dot{q}_2} = 0.035$ . Since the delay time of the controller is  $\tau = 0.1$  in our calculations, on average, the first controller  $u_1(t, \tau)$  corrects the stick movement more slowly than the delay time, whereas the second controller  $u_2(t, \tau)$  performs the corrections in a shorter



FIGURE 8. Short-time cross-correlation coefficient at  $t = 36$ .

time than the delay time. Regarding  $\hat{\tau}_{q_1}$ ,  $\hat{\tau}_{q_2}$  as the tracking ability of the controller, the second controller can track the stick movement  $0.105/0.035 = 3$  times faster than the first controller, which indicates that symmetrically placed controllers  $u_1$  and  $u_2$  having the same specifications can develop asymmetric tracking abilities over short time scales.

The peak points  $\hat{\tau}_{\dot{x}}$  and  $\hat{\tau}_{\dot{q}_i}$  ( $i = 1, 2$ ) are plotted in Fig.9 as a function of time  $t$ . The plots are numerically constructed from single realizations of numerical solutions of (3) and (5). The peak points randomly fluctuate over time, forming intermittent clusters of points. The sensitive region in which the peak point is smaller than the delay time is confirmed to be of sufficient length for physical observations. However, the effects of coupling are not clearly observable in Fig.9. Therefore, the differences between the results (a), (b), and (c) in Fig.9 in these plots are slight.

In order to evaluate the effects of coupling on tracking ability, the probability densities of the peak points  $\hat{\tau}_{\dot{x}}$  and  $\hat{\tau}_{\dot{q}_1}$  are shown in Fig.10 as averaged over 100 realizations over the time interval  $[0, 1200]$  of the numerical solutions of (3) and (5). The results for  $\hat{\tau}(\dot{q}_2)$  are omitted because it is quite similar to that for  $\hat{\tau}(\dot{q}_1)$ . It is clearly observed in Fig.10 that the density of coupled balancing, represented as small rectangles, produces a simple peak, which is 38% higher than that for single balancing, where the peak is placed at a time scale of  $\hat{\tau}$ , which is 20% shorter than that for single balancing.

Based on these results, it can be concluded that the mechanical coupling structure increases the probability of the occurrence of faster corrective movements and improves the tracking ability of the controllers. One possible interpretation could be that this noise-induced sensitivity is a version of the stochastic resonance [13] (SR), a random phenomenon modeled by a heavily damped particle moving randomly in a double well potential. The SR approach has been applied to single human balancing [14]. However, the SR approach to the coupled human balancing remains unclear and will be discussed later herein.

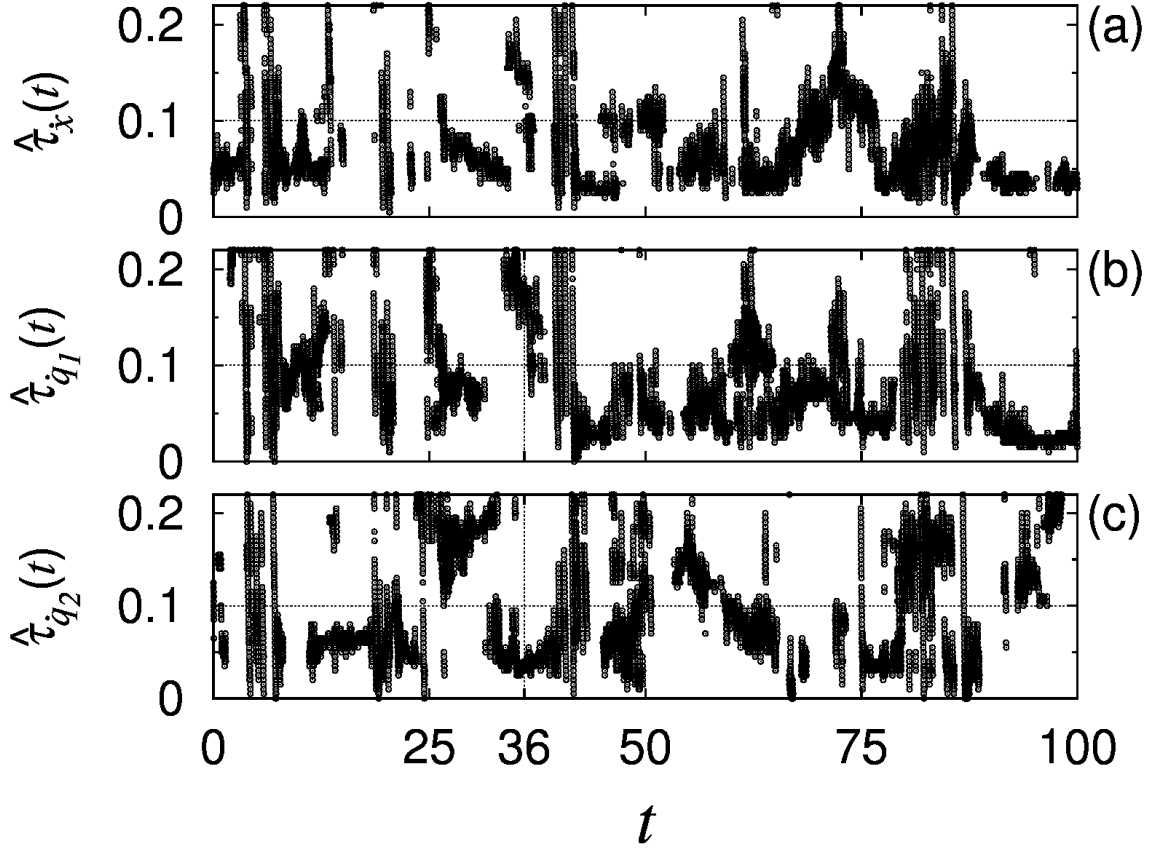


FIGURE 9. First peak points  $\hat{\tau}_{\dot{x}}(t)$ ,  $\hat{\tau}_{\dot{q}_1}(t)$ , and  $\hat{\tau}_{\dot{q}_2}(t)$  of the short-time cross-correlation coefficients  $R(\dot{x}_T, \dot{x}_M; \tau)$ ,  $R(\dot{q}_T, \dot{q}_{M1}; \tau)$ , and  $R(\dot{q}_T, \dot{q}_{M2}; \tau)$ , respectively, at time  $t$ .

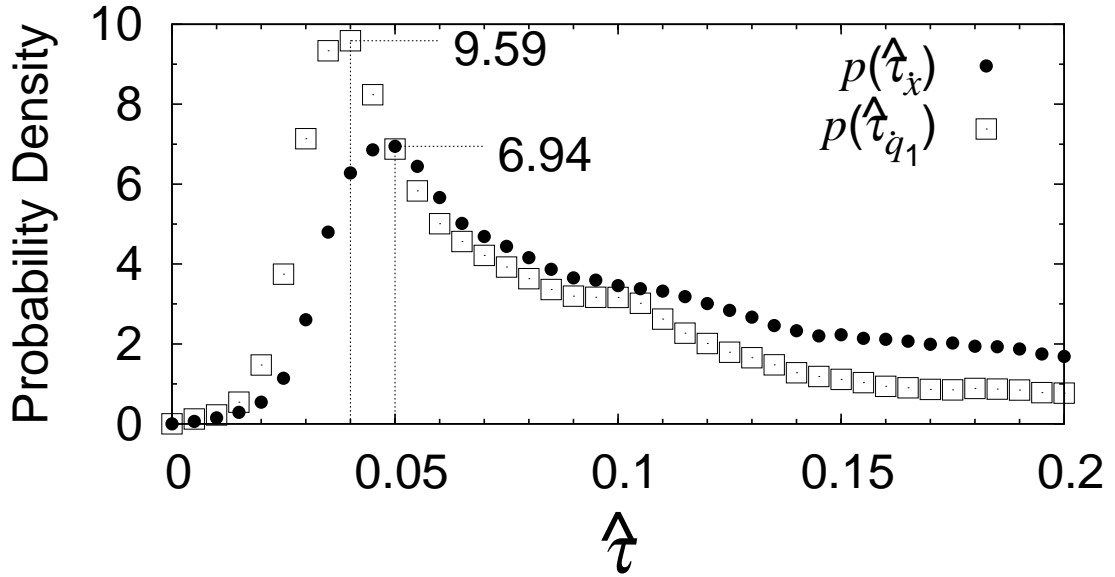


FIGURE 10. Probability densities of the first peak point  $\hat{\tau}_{\dot{x}}(t)$  for the single case and  $\hat{\tau}_{\dot{q}_1}(t)$  for the coupled case as constructed from 100 samples in the time interval  $t \in [0 : 1200]$ .

#### 4. Experiment of Coupled Visuomotor Tracking on a Computer Screen.

**4.1. Experimental setup.** We perform an experiment in which the numerical pseudo-neural controllers in (5) are replaced by natural human balancing tasks, as shown in Fig.11(a). In practice, the variable  $x_M$  in the single model (3) is replaced with the movement of a mouse manipulated by a subject, and  $q_{M1}$  and  $q_{M2}$  in (5) are replaced by those of two subjects. Each subject is presented with combinations of thick and thin lines on a computer screen, as shown in Fig.11(b). The thick lines represent the upper ends  $x_T$  and  $q_{Ti}$  as calculated from the numerical models (3) and (5), while the thin lines represent the lower ends  $x_M$  and  $q_{Mi}$  manipulated by the subjects. The screen resolution is  $1,200 \times 600$  (pixels), where the range of the displacement  $[-3, 3]$  in the numerical model maps to the horizontal range of pixels  $[1, 1,200]$  on the screen. The movements performed by the subjects  $x_M$  and  $q_{Mi}$  are recorded and substituted into the numerical models (3) and (5) with a sampling rate of 50 Hz, and the set of lines on the screen is animated at the same rate.

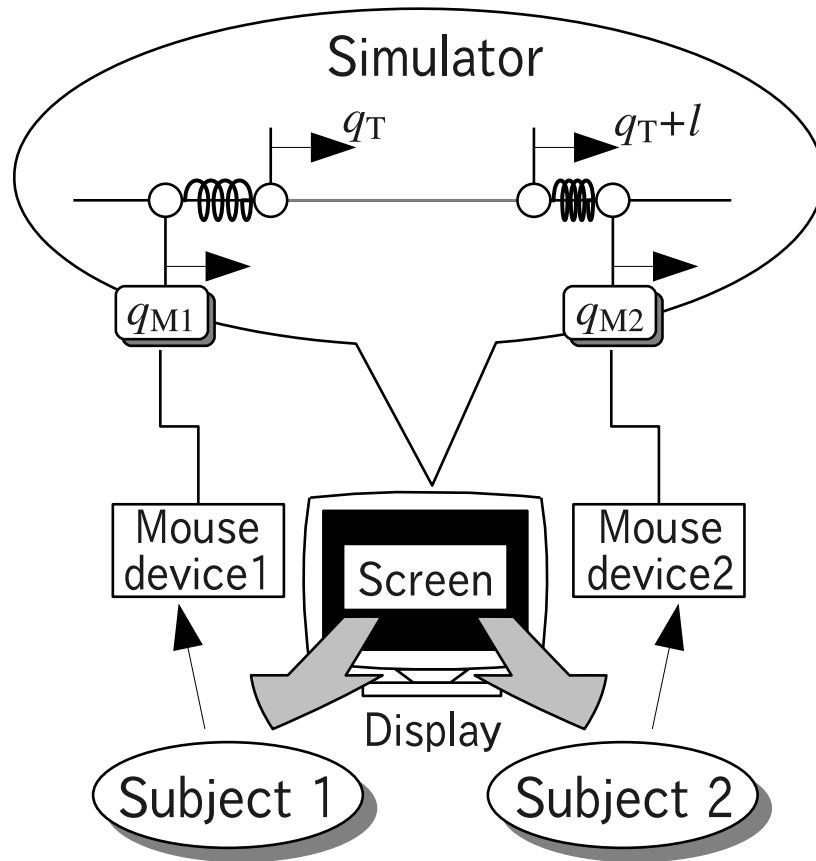
The experimenter issues the following instructions to the subjects:

- Each subject should collaborate with his/her partner in order to maintain the assigned pendulum, provided as an overhead view on the computer screen, in the upright position by manipulating the lower end of the pendulum, which is represented as a thin line.
- The upper ends, represented as thick lines, are assumed to be connected by a rigid rod in such a way that a constant distance is maintained between the thick lines.
- The experiment begins after a countdown performed by the experimenter, and ends after ten minutes or when any of the lines leaves the visible range.
- The subject can abort the experiment at anytime.

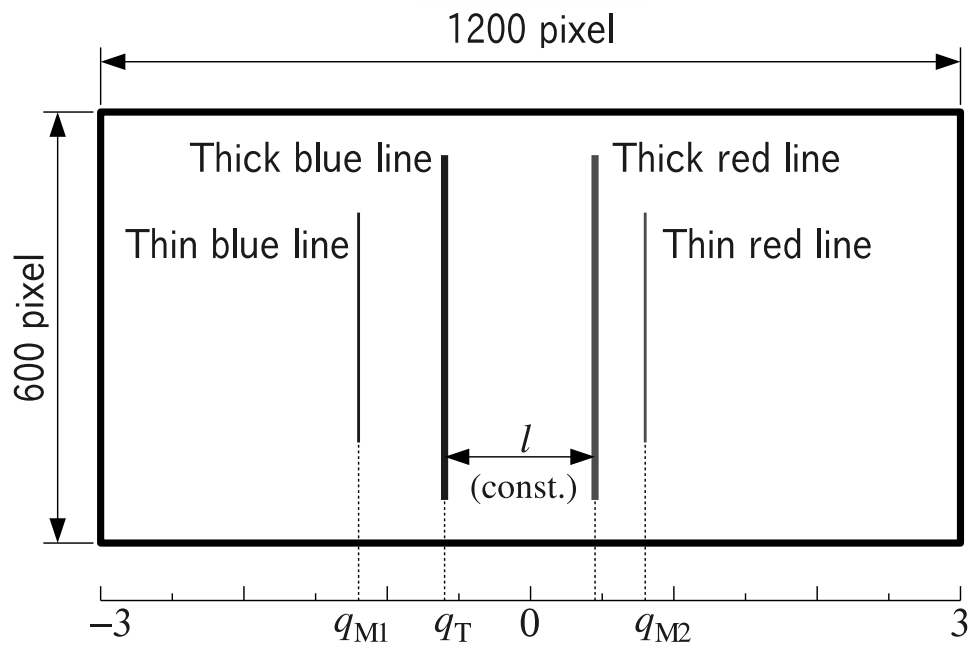
According to these instructions, after the countdown, the numerical simulation is started and the experiment begins. The experiment ends after ten minutes or when any of the lines  $x_T$ ,  $q_{Ti}$ , and  $x_M$ ,  $q_{Mi}$  leaves the visible range  $[-3, 3]$ . The initial positions of the animated lines, i.e., the initial values of the models, are set to  $x_T(0) = -0.5$ ,  $q_{M1}(0) = -0.6$ ,  $q_{M2}(0) = 0.6$ ,  $\dot{x}_T(0) = \dot{x}_M(0) = 0$ ,  $q_T(0) = -0.5$ ,  $q_{M1}(0) = -0.6$ ,  $q_{M2}(0) = 0.6$ , and  $\dot{q}_T(0) = \dot{q}_{M1}(0) = \dot{q}_{M2}(0) = 0$ . The model parameters are chosen to be  $\alpha = \beta = 21$ ,  $\gamma = 50$ , and  $l = 1$ .

The six subjects were healthy volunteers aged 21 to 24 years. The experiments were performed according to the principles of the Declaration of Helsinki and informed consent was obtained. The experimental protocol was approved by the Bioethics Committee of Utsunomiya University. The subjects were labeled A, B, C, D, E, and F, and three pairs (A,B), (C,D), and (E,F) are considered in the coupling task.

**4.2. Experimental results.** First, we focus on subjects A and B and the pair (A,B). Figure 12 shows the experimental results for single balancing performed independently by subjects A and B. The thick line, which corresponds to the velocity  $\dot{x}_T$  of the target (the upper end of the stick), slightly precedes the thin line, which corresponds to the subject's velocity  $\dot{x}_M$ , due to a combination of time delays from neural reflexes and computer processing. Moreover, for the case in which balancing is performed by both subjects, the power spectrum  $S(\omega)$  of the balancing error  $\Delta x$  exhibits a power law behavior typical of neural controllers, which have two different power laws with an exponent of  $\approx -1/2$  in the lower-frequency range [6].



(a) Experimental device.



(b) Screen design.

FIGURE 11. Experimental setup of the coupled human balancing tasks.

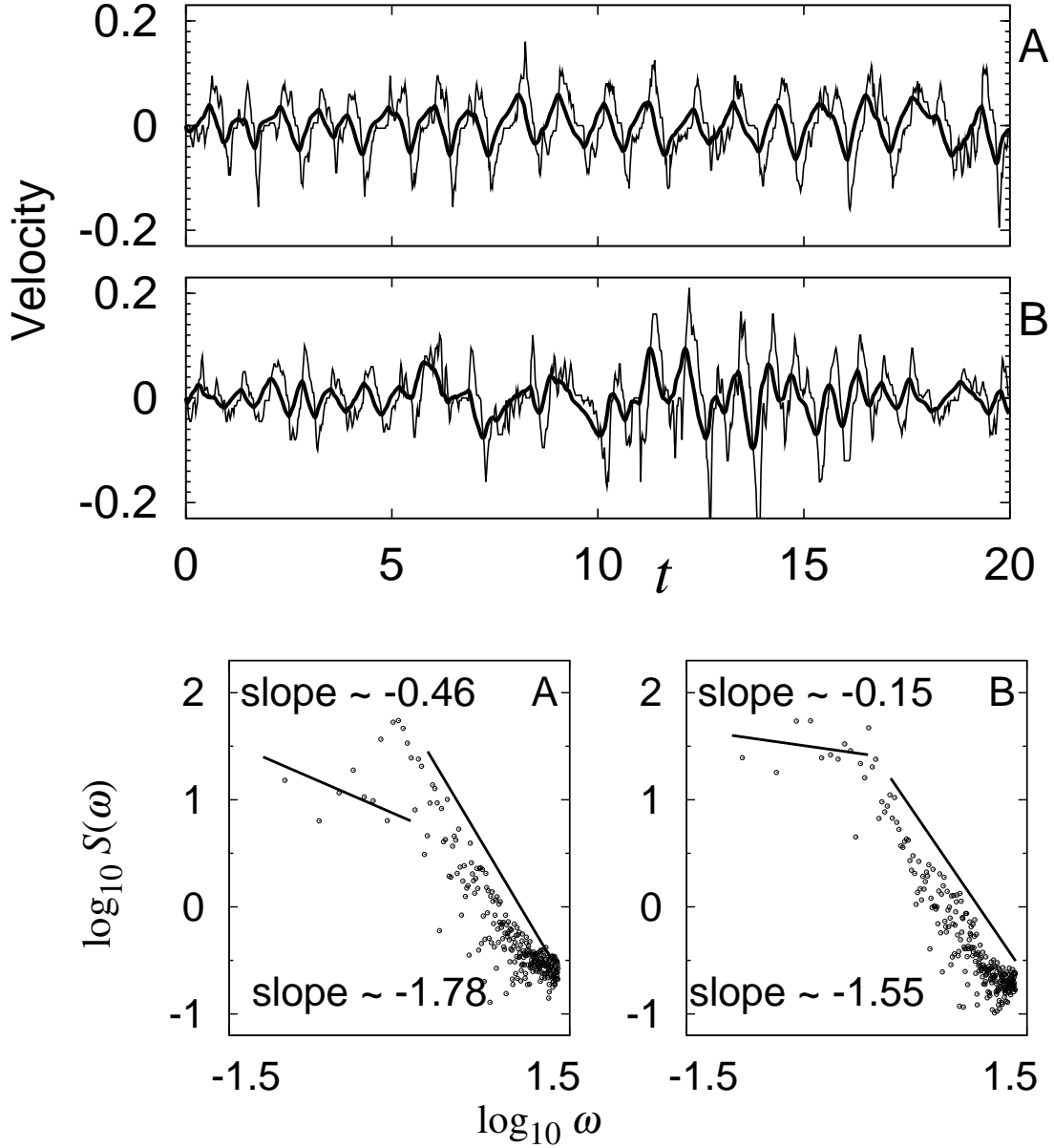


FIGURE 12. Experimental velocities of the target  $\dot{x}_T$  (thick line) and of the subject's movement  $\dot{x}_M$  (thin line), and power spectra of the balancing error  $\Delta x$  for single balancing performed independently by subjects A and B.

On the other hand, Fig.13 shows the experimental results for the case in which the same subjects are coupled by a rigid rod of length  $l$  in the numerical model. Note that, as a result of the equalities (4), the velocities of both targets (thick lines) coincide. The thick line, which corresponds to the target velocity  $\dot{q}_T$ , slightly precedes the thin line, which corresponds to the velocities  $\dot{q}_{M1}$  and  $\dot{q}_{M2}$  of the subject, and the balancing errors  $\Delta q_1$  and  $\Delta q_2$  are governed by a power law having an exponent of  $\approx -1/2$  in the lower-frequency range. Based on these results, the mechanical coupling structure between the two balancing tasks maintains the time-delay and scaling-law properties typical of the independently performed single balancing tasks.

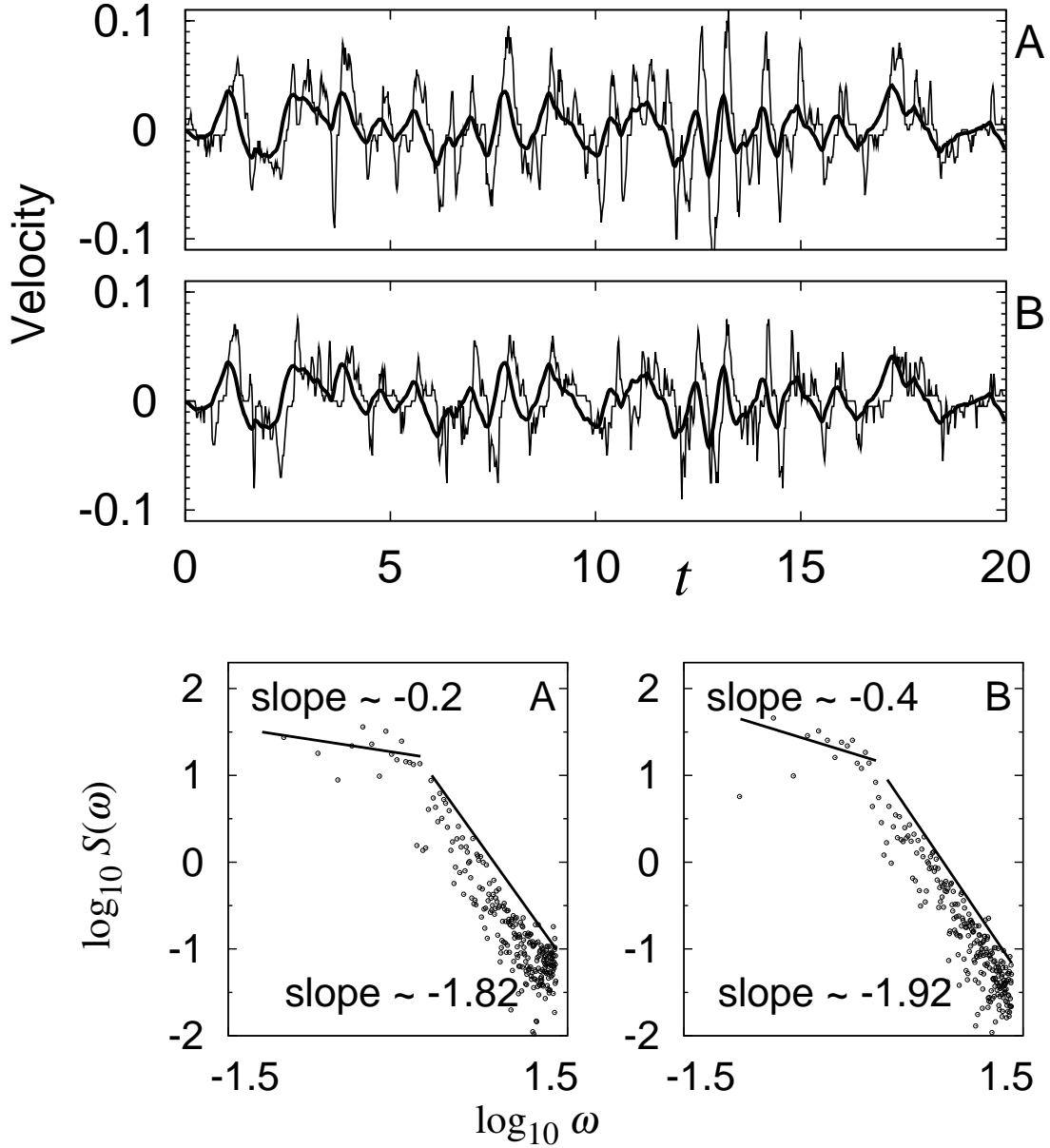


FIGURE 13. Experimental velocities of the target  $\dot{q}_T$  (thick line) and of the subject's movement  $\dot{q}_{Mi}$  (thin line), and power spectra of the balancing error  $\Delta q_i$  for coupled balancing by the pair of subjects A ( $i = 1$ ) and B ( $i = 2$ ).

**4.3. Effects of coupling on stability and sensitivity.** As discussed in Section 3.3, the correlation time (the first dominant peak in STCC) allows us to evaluate the sensitivity of the corrective movements of the subjects, i.e., the tracking ability of the subjects. The experimental correlation times for single balancing performed independently by the two subjects (denoted as A and B) are shown in Fig.14 as peak points  $\hat{\tau}_{\dot{x}_T} = 0.14, 0.12$  of STCC. The differences between the correlation times become slightly larger when the mechanical coupling structure is placed between the two balancing tasks, as shown in Fig.15, i.e.,  $\hat{\tau}_{\dot{x}_T} = 0.12, 0.18$ . The correlation times obtained from different trials of the experiment and their averages are listed in Table

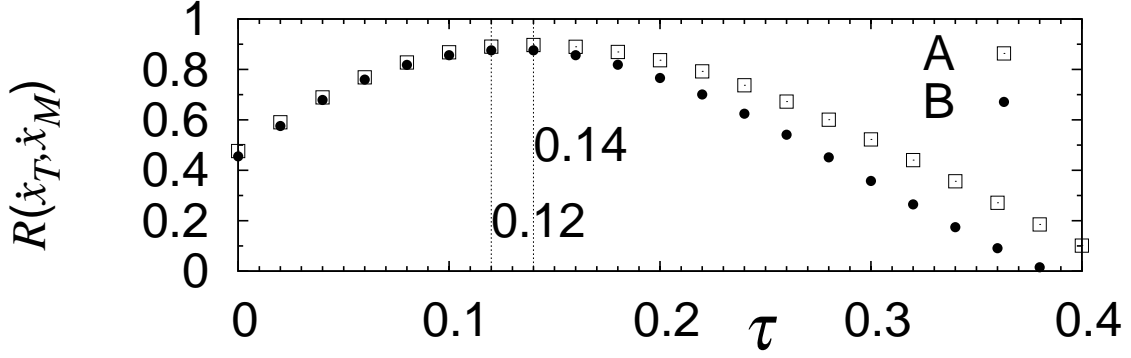


FIGURE 14. Experimental short-time cross-correlation coefficients  $R$  for single balancing performed independently by subjects A and B.

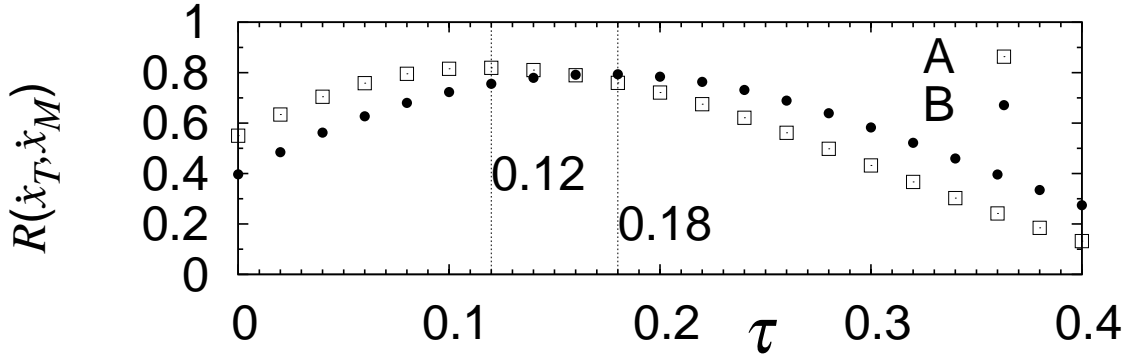


FIGURE 15. Experimental short-time cross-correlation coefficients  $R$  for coupled balancing performed by pair (A,B).

1. The averages in Table 1 show that the coupling structure increases the individual differences between the subjects. In other words, the single balancing tasks yield similar tracking abilities ( $\langle \hat{\tau} \rangle = 0.132, 0.136$ ), whereas the tracking abilities become asymmetric ( $\langle \hat{\tau} \rangle = 0.128, 0.168$ ) when coupled by the mechanical structure. Similarly, Table 2 lists the RMS of the balancing errors and their averages for estimating the stabilities of the balancing. The averages in Table 2 indicate that the coupling has the opposite effect on the RMS, as compared with the STCC, i.e., the coupling structure decreases the individual differences in the RMS of the balancing errors from  $\langle \text{RMS} \rangle = 3.62$  and  $5.34$  for the single task to  $\langle \text{RMS} \rangle = 3.02$  and  $2.50$  for the coupled task.

The results in Table 1 and 2 imply that the coupling structure increases the individual differences between the tracking abilities (STCC), while decreasing those of the balancing stabilities (RMS). This effect on the six subjects can be seen in Fig.16, which shows experimental plots of the correlation time  $\tau$  versus the RMS of the balancing errors over all trials of the single balancing tasks performed by subjects A, B, C, D, E, and F and the coupled balancing tasks performed by pairs (A,B), (C,D), and (F,D). The plots with filled triangles indicate the results for the single tasks, and the plots with rectangles indicate the results for the coupled tasks. The oval is centered at the average point of the corresponding plots and the radii in the horizontal and vertical directions represent the standard deviations of the correlation time and of the RMS of

TABLE 1. Correlation times at different trials for pair (A,B).

Subject	Index of trial					Average $\langle \hat{\tau} \rangle$
	1	2	3	4	5	
Single:						
A	0.12	0.14	0.14	0.12	0.14	0.132
B	0.14	0.12	0.14	0.14	0.14	0.136
Coupled:						
A	0.12	0.12	0.12	0.12	0.16	0.128
B	0.18	0.16	0.16	0.18	0.16	0.168

TABLE 2. RMS of the balancing errors at different trials for pair (A,B).

Subject	Index of trial					Average $\langle \text{RMS} \rangle$
	1	2	3	4	5	
Single:						
A	2.4	2.9	3.8	5.5	3.5	3.62
B	4.9	4.9	5.8	5.0	6.1	5.34
Coupled:						
A	2.9	3.5	2.4	3.9	2.4	3.02
B	2.4	2.8	2.6	2.7	2.0	2.50

balancing errors, respectively. A comparison of the single tasks for the solid oval with the coupled tasks for the dashed oval reveals that the coupling structure decreases the individual differences in correlation time, while increasing the individual differences in the RMS. This result statistically confirms the coupling effect arising in the two subjects, as shown in Table 1 and 2.

One possible explanation for these effects of coupling on the individual differences might be the separation of roles assumed by the subjects in the case that requires cooperation. However, similar asymmetrical properties can arise in the numerical controller  $u_i(t, \tau)$  in the second equation of (5), which has no ability to cooperate. Moreover, the numerical controllers provide feedback of the combination of their own past states and the shared state, i.e.,  $\Delta q_i = q_T - q_{Mi}$ , in the following form:

$$u_i = u_i(\Delta q_i) \quad \left( = \beta R_i(t) \Delta q_i(t - \tau) \text{ in (5)} \right). \quad (9)$$

In contrast, the human subjects can also receive visual feedback of their partner's state via the shared computer screen in Fig.11, and, as a result, their controller model may appear to have the following structure:

$$u_i = u_i(\Delta q_1, \Delta q_2) \quad (i = 1, 2). \quad (10)$$

Developing precise descriptions of such a human controller model will provide the first step toward exploring the coupling effects, such as the changes in the individual differences. For this purpose, it appears that approaches based on learning theory and evolutionary methods [15,16] will be helpful. However, a detailed explanation of these effects is beyond the scope of the present paper and will be discussed elsewhere.

**5. Conclusion.** Coupled human balancing tasks are investigated based on pseudo-neural controllers modeled using time-delayed feedback with random gain. It is shown



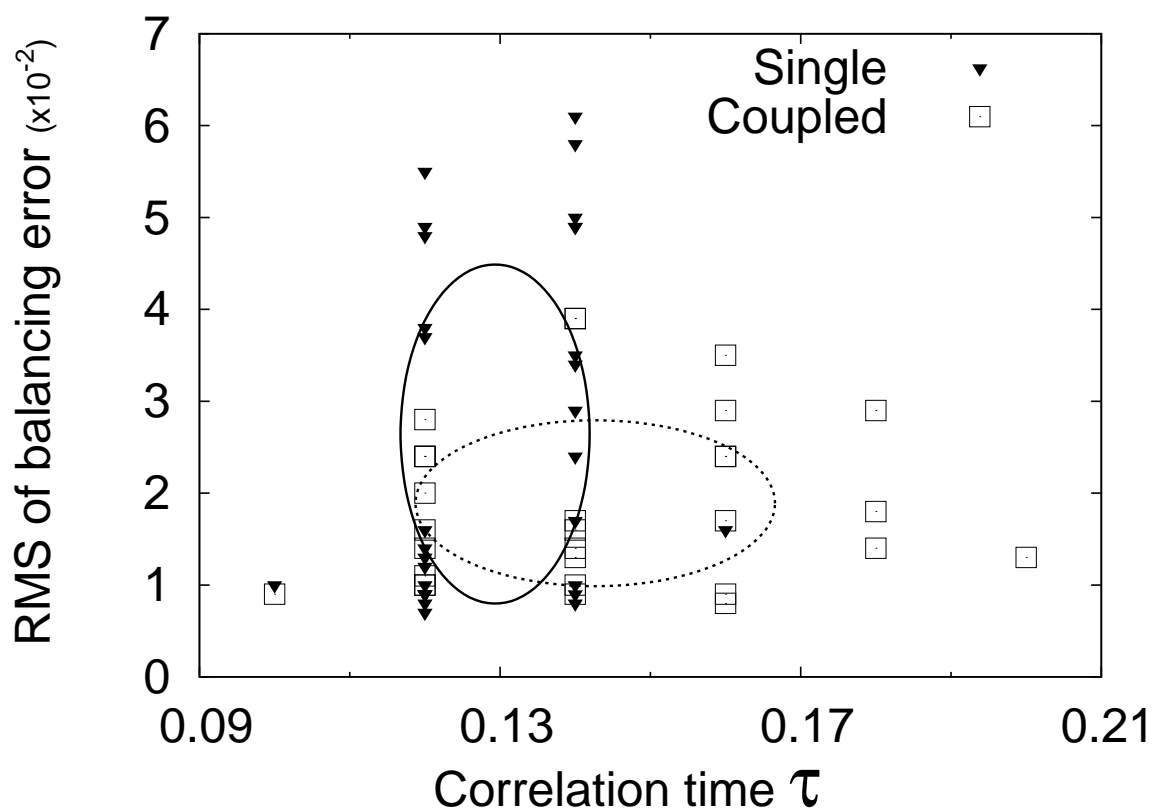


FIGURE 16. Experimental plots of the correlation time  $\tau$  versus the RMS of the balancing errors over all trials of the single balancing tasks performed by subjects A, B, C, D, E, and F and the coupled balancing tasks performed by pairs (A,B), (C,D), and (F,D).

numerically that, compared with the case of single balancing tasks, the coupling structure increases the stability against balancing errors in terms of both amplitude and velocity and improves the tracking ability of the controllers. We then perform an experiment in which the pseudo-neural controller in the numerical model is replaced with natural human balancing tasks carried out using computer mice. The results reveal that the mechanical coupling structure increases the individual differences in the tracking abilities between the subjects, while decreasing the individual differences in the stabilities of the balancing errors. The proposed model and experimental method are expected to provide the simplest means by which to understand the cooperative behavior between humans sharing mechanical contacts and to provide new insight into welfare engineering and related fields. In the future, we intend to perform model identification of human visuomotor tracking tasks in order to characterize the trade-off mechanism between tracking abilities and stabilities produced by coupled human subjects.

## REFERENCES

- [1] K. Sigmund and J. Hofbauer. *Evolutionary Games and Population Dynamics*. Cambridge University Press, 1998.
- [2] H. Asama, T. Fukuda, T. Arai, and I. Endo, editors. *Distributed Autonomous Robotic Systems 2*. Springer-Verlag, 1996.
- [3] Katsutoshi Yoshida and Hiroki Ohta. Coupled inverted pendula model of competition and cooperation. *Journal of System Design and Dynamics*, vol.2, no.3, pp.727–737, 2008.

- [4] Ming-Liang Li, Yu-Kuei Chiu, Yi-Nung Chung, and Chao-Hsing Hsu. A dynamic controlling scheme for a tracking system. *ICIC Express Letters*, vol.3, no.2, pp.219–223, June 2009.
- [5] Chien-Wen Lai, Pei-Kun Chen, Yi-Nung Chung, and Chao-Hsing Hsu. Applying adaptive estimator to maneuvering tracking system. *ICIC Express Letters*, vol.3, no.3, pp.327–432, September 2009.
- [6] Juan Luis Cabrera and John G. Milton. On-off intermittency in a human balancing task. *PRL*, vol.89, no.15, pp.158702, October 2002.
- [7] Sue Ann Campbell, R. Edwards, and P. van den Driessche. Delayed coupling between two neural network loops. *S.I.A.M. Journal on Applied Mathematics*, vol.65, no.1, pp.316–335, 2004.
- [8] Sue Ann Campbell, I. Ncube, and J. Wu. Multistability and stable asynchronous periodic oscillations in a multiple-delayed neural system. *Physica D*, vol.214, pp.101–119, 2006.
- [9] Shankar C. Venkataramani, Thomas M. Antonsen Jr., Edward Ott, and John C. Sommerer. On-off intermittency: Power spectrum and fractal properties of time series. *Physica D*, pp.66–99, 1996.
- [10] Juan Luis Cabrera and John G. Milton. Human stick balancing: Tuning lévy flights to improve balance control. *Chaos*, vol.14, no.3, pp.691–698, 2004.
- [11] R. Bormann, J.-L. Cabrera, J. G. Milton, and C. W. Eurich. Visuomotor tracking on a computer screen—an experimental paradigm to study the dynamics of motor control. *Neurocomputing*, vol.58, no.60, pp.517–523, 2004.
- [12] K. Matsumoto and I. Tsuda. Noise-induced order. *Journal of Statistical Physics*, vol.31, no.1, pp.87–106, April 1983.
- [13] Luca Gammaitoni, Peter Hänggi, Peter Jung, and Fabio Marchesoni. Stochastic resonance. *Reviews of Modern Physics*, vol.70, no.1, pp.223–287, January 1998.
- [14] Attila A. Priplata, Benjamin L. Patritti, James B. Niemi, Richard Hughes, Denise C. Gravelle, Lewis A. Lipsitz, Aristidis Veves, Joel Stein, Paolo Bonato, , and James J. Collins. Noise-enhanced balance control in patients with diabetes and patients with stroke. *Annals of Neurology*, vol.59, no.1, pp.4–12, November 2006.
- [15] Genci Capi. Application of recurrent neural controllers for robot complex task performance. *International Journal of Innovative Computing, Information and Control*, vol.5, no.5, pp.1171–1178, May 2009.
- [16] Genci Capi and Shinichiro Kaneko. Evolution of neural controllers in real mobile robots for task switching behaviors. *International Journal of Innovative Computing, Information and Control*, vol.5, no.11, pp.4017–4024, November 2009.